Modeling Advanced Magnetoresistive Memories

Viktor Sverdlov
Christian Doppler Laboratory for Nonvolatile Magnetoresistive Memory and Logic
Institute for Microelectronics, TU Wien
Vienna, Austria
sverdlov@iue.tuwien.ac.at

Bernhard Pruckner
Christian Doppler Laboratory for Nonvolatile Magnetoresistive Memory and Logic
Institute for Microelectronics, TU Wien
Vienna, Austria
pruckner@iue.tuwien.ac.at

Nils Petter Jørstad
Christian Doppler Laboratory for Nonvolatile Magnetoresistive Memory and Logic
Institute for Microelectronics, TU Wien
Vienna, Austria
jorstad@iue.tuwien.ac.at

Mario Bendra
Christian Doppler Laboratory for Nonvolatile Magnetoresistive Memory and Logic
Institute for Microelectronics, TU Wien
Vienna, Austria
bendra@iue.tuwien.ac.at

Siegfried Selberherr
Institute for Microelectronics, TU Wien
Vienna, Austria
selberherr@iue.tuwien.ac.at

Wolfgang Goes
Silvaco Europe Ltd.
Cambridge, United Kingdom
wolfgang.goes@silvaco.com

***Abstract*—Nonvolatile CMOS-compatible spin-transfer torque (STT) and spin-orbit torque (SOT) magnetoresistive random access memories (MRAMs) possess high speed and endurance as well as long retention compared to their competitors. Advanced MRAM devices are composed of multiple magnetic layers separated by tunnel barriers and non-magnetic metallic spacers. To efficiently model magnetization dynamics in complex, multilayered structures, we use a coupled spin and charge transport approach, which accurately captures the spin accumulation and the torques acting on ferromagnetic layers. Appropriate boundary conditions at the interfaces are applied to determine the spin and charge transport in metallic spin valves and magnetic tunnel junctions. We demonstrate the versatility of our approach by applying it to evaluate operation in ultra-fast multilayer STT-MRAM, efficient magnetic field-free switching in SOT-MRAM with a heavy metal/ferromagnetic SOT stack, as well as a magnetization control in strained noncollinear antiferromagnet Mn_3Sn. By combining an Mn_3Sn layer with a ferromagnetic layer, electrical control over magnetization is achieved, opening perspectives for future field-free SOT-MRAM devices.**

Keywords— Spin and charge drift-diffusion, spin torques, magnetic tunnel junctions, TCAD, STT-MRAM, composite free layer, SOT-MRAM, field-free switching, noncolinear antiferromagnets.

I. INTRODUCTION

The key element of a magnetoresistive random access memory cell is a magnetic tunnel junction (MTJ) [1], [2], [3], which is composed of two ferromagnets separated by a tunnel barrier. Its resistance depends on the relative orientation of the ferromagnetic contacts: The resistance is high for antiparallel (AP) and low for parallel (P) configuration. The ratio of the resistance difference in the AP and P configuration to the resistance in the P configuration is the tunnel magnetoresistance ratio. For CoFeB|MgO|CoFeB cylindrical pillars currently employed for advanced MTJs with perpendicular magnetization (p-MTJs), the magnetoresistance ratio reaches a few hundred percent at room temperature [4], [5]. Binary information stored in an MTJ configuration by assigning a logical zero to an MTJ in parallel and a logical one to the antiparallel state can be read by sensing the resistance. The typical resistance of an MTJ is comparable to that of a MOSFET. This makes RAM electrically compatible with CMOS circuitry, eliminating the need for additional amplifiers otherwise required to convert the spin (magnetization) orientations into electric (current, voltage) signals.

The information is written by creating the required parallel or antiparallel MTJ configuration. The orientation of one of the MTJ's ferromagnets is fixed, while the magnetization of another, free, ferromagnetic layer can be flipped. In STT-MRAM, the free layer (FL) magnetization is manipulated by the spin-transfer torque generated by the spin-polarized current run through the MTJ. The spin polarization of the current passing through the fixed ferromagnetic reference layer (RL) is transferred to the magnetization of the FL [6], [7]. This spin-transfer torque causes magnetization switching, if the current density is sufficiently large to overcome the damping. To flip the free layer and alternate the magnetic configuration, the current flow is inverted.

STT-MRAM is fast (1-10 ns) and possesses high endurance (10^{12}). It also requires fewer additional masks for fabrication compared to flash memory. STT-MRAM solutions implemented with 16nm FinFET [8] for last-level caches and 16 nm FD SOI [9] technology for embedded MRAM are already available. A roadmap for STT-MRAM [10] institutionalizes that it is scalable beyond flash memory limits as a highly reliable embedded memory for automotive applications compatible with the 8 nm logic node [11]. To further reduce the MTJ footprint to single-digit nanometer size, the FL is split into several elongated nanopillars with MgO layers in between [12].

To further increase the operating speed, an additional fixed ferromagnetic RL separated from the FL by a non-magnetic metal spacer (NMS) is included [13]. Double spin-torque magnetic tunnel junction (dsMTJ) structures [13] with two RLs reduce the switching current by a factor of two, however, the current is still running through the MTJ. In STT-MRAM, increasing the current is the only option to meet the requirements for higher-level caches. Spin-orbit torque (SOT) MRAM is an electrically addressable, nonvolatile memory with high speed and endurance suitable for replacing SRAM in hierarchical multi-level processor memory.

SOT provides a fast and efficient way to manipulate the magnetization [14]. These devices take advantage of the strong spin-orbit coupling in the bulk or at the interfaces of heavy metal (HM) layers to generate spin-polarized currents. When injected into an adjacent ferromagnetic FL of an MTJ grown on the HM, the spin currents exert torques

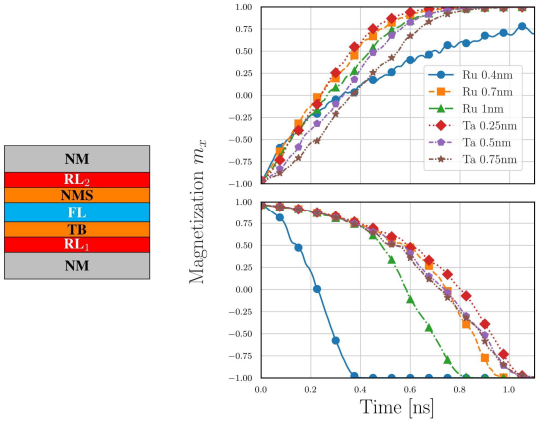

Fig.1. **Left**: dsMTJ multilayer design. The color coding represents RLs in red, the FL in cyan, the tunnel barrier and the NMS in orange, HL in purple, and non-magnetic contacts in gray. **Right**: Switching performance for dsMTJ multilayer devices utilizing a Ru/Ta-NMS under varying NMS thicknesses and IEC strength.

on the FL. The spin currents are generated through the spin Hall effect (SHE) in the HM and through the Rashba-Edelstein effect (REE) at the HM/FL interface [15].

Modeling advanced MRAM cells requires an accurate evaluation of spin currents and torques in MTJs with composite FLs and several RLs. Here, we extend the coupled spin-charge drift-diffusion approach to evaluate spin torques in multilayered structures [16] in the presence of the interfacial exchange coupling [17] and to account for the torques generated by the SHE and REE. We confirm the versatility of our approach by applying it to multilayer ultra-fast STT-MRAM, efficient magnetic field-free switching in SOT-MRAM with a HM/ferromagnetic SOT stack, temperature-assisted switching in a two-terminal SOT-MRAM as well as a to magnetization control in strained noncollinear antiferromagnet Mn_3Sn.

II. Modeling Ultra-fast Multilayer STT-MRAM

The advancement of sub-nanosecond MTJs is crucial for next-generation nonvolatile memory, impacting computing, automotive, and storage industries. DsMTJs [13] enhance traditional MTJs by integrating an additional RL separated by a NMS, improving switching efficiency and performance.

The dsMTJ stack is simulated in a form, as shown in Fig.1 (left), where the RL is treated as a single layer. We employ our fully three-dimensional finite element modeling approach [16], [18] to evaluate these modifications, combining the drift-diffusion method with the Landau-Lifshitz-Gilbert equation:

$$\frac{\partial \mathbf{m}}{\partial t} = -\gamma\mu_0 \mathbf{m}\times\mathbf{H}_{\text{eff}} + \alpha\mathbf{m}\times\frac{\partial \mathbf{m}}{\partial t} + \frac{1}{M_S}\mathbf{T_S} \qquad (1)$$

Here $\mathbf{m}=\mathbf{M}/M_S$ is the position and time-dependent normalized magnetization, M_S is the saturation magnetization, α is the Gilbert damping constant, γ is the gyromagnetic ratio, μ_0 is the vacuum permeability. The effective field $\mathbf{H}_{\text{eff}}$ includes the magnetic anisotropy field, the exchange field, as well as the demagnetization and stray fields. The coupled spin and charge drift-diffusion (DD) method accurately describes the spin accumulation $\mathbf{S}$ and the corresponding torques $\mathbf{T_S}$ acting on the magnetization. In order to describe the STT acting on the magnetization in a

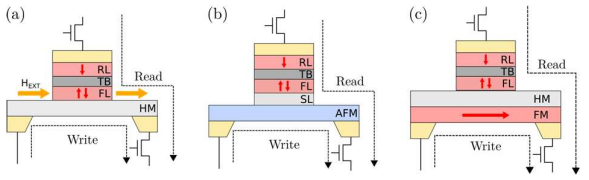

Fig.2 SOT-MRAM cells consisting of FL and RL, separated by a TB, sitting on top of the HM with SHE/REE (**a**) and on an antiferromagnetic (AFM) layer with the magnetic spin Hall effect (**b**). A spacer layer (SL) is introduced between the FL and the HM to mitigate the exchange coupling. **c**: An SOT-MRAM cell with an additional in-plane ferromagnetic layer under the HM. Cell information read and write paths are shown for convenience.

nanometer-sized multilayer MTJs shown in Fig.1 (left) continuous boundary conditions for the spin accumulation and the spin current densities [17] are employed at the interfaces between a ferromagnet and an NMS. For a given charge current density $\mathbf{J_C}$ the in-plane Slonczewski interface polarization parameters P_{RL}, P_{FL} complemented with the out-of-plane factors P_{RL}^{η}, P_{FL}^{η} define the spin current density floating through the tunnel barrier:

$$\mathbf{J_{S,TB}} = -\frac{\mu_B}{e}\frac{\mathbf{J_C}\cdot\mathbf{n}}{1+P_{RL}P_{FL}\mathbf{m_{RL}}\cdot\mathbf{m_{FL}}}\Big(P_{RL}\mathbf{m_{RL}} + P_{FL}\mathbf{m_{FL}} + \frac{1}{2}\big(P_{RL}P_{RL}^{\eta} - P_{FL}P_{FL}^{\eta}\big)\mathbf{m_{RL}}\times\mathbf{m_{FL}}\Big) \qquad (2)$$

Here $\mathbf{m_{RL}}$ and $\mathbf{m_{FL}}$ are the normalized magnetization vectors of the RL and FL at the TB interfaces, respectively.

We focus on the role of interlayer exchange coupling (IEC) in enhancing dsMTJ switching performance (Fig.1). IEC in metallic valves is influenced by NMS thickness and exhibits oscillatory ferromagnetic (FM) to antiferromagnetic (AFM) character based on RKKY interactions.

Fig.1, right panel, shows the impact of different NMS materials and their resulting IEC on the dsMTJ performance. Optimal performance is achieved with a Ru NMS at 1 nm thickness, exhibiting AFM coupling of 0.65 mJm^{-2}. For a Ta NMS, the best performance was observed at 0.25 nm thickness with FM coupling of 0.4 mJm^{-2}. The fastest switching from the anti-parallel to the parallel state is achieved with a Ru NMS at 0.4 nm, corresponding to an AFM coupling of 2.1 mJm^{-2} (Fig.1, right panel). A Ru NMS is characterized by a longer spin-flip length of 4 nm and demonstrates better performance compared to a Ta NMS, with a shorter spin-flip length of 1.7 nm, because of a slower spin accumulation decay and larger torques, correspondingly.

III. Spin-Orbit Torques for Advanced MRAM

Spin-orbit torque (SOT) provides rapid and energy-efficient manipulation of magnetic states in emerging SOT-MRAM [14] (Fig.2). SOT, generated through the SHE and REE at the interface in NM/ferromagnet FL bilayers (Fig.2a), has proven successful in switching logical states in SOT-MRAM. Torques $\mathbf{T_S}$ acting on the FL magnetization $\mathbf{m}$ are caused by the nonequilibrium spin accumulation $\mathbf{S}$ [20]:

$$\mathbf{T_S} = -\frac{D_e}{\lambda_j^2}\mathbf{m}\times\mathbf{S} - \frac{D_e}{\lambda_\varphi^2}\mathbf{m}\times(\mathbf{m}\times\mathbf{S}) \qquad (3)$$

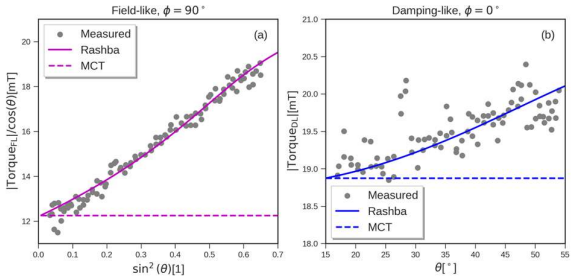

Fig.3. Angular dependence of SOTs in a Pt(3 nm)/Co(0.6 nm) bilayer with a 0.38×10^{12} Am^{-2} electrical current along the x-direction. The torques were computed using a spin drift-diffusion model with boundary conditions for interfacial SOC and fitted to experimental data [21]. The field-like (**left**) and damping-like (**right**) torques could be reproduced only, if the interracial REE is considered.

Here, λ_J is the exchange length, and λ_φ is the spin dephasing length. The spin accumulation is obtained with the coupled spin and charge drift-diffusion approach [20] generalized to include the SHE via the spin current $\overline{\mathbf{J}_\mathbf{S}}$ in HM:

$$\overline{\mathbf{J}_\mathbf{S}} = -D_e \boldsymbol{\nabla}\mathbf{S} - \theta_{SH}\boldsymbol{\varepsilon}\mathbf{J}_\mathbf{C} \qquad (4)$$

$\boldsymbol{\varepsilon}$ is the unit antisymmetric tensor and θ_{SH} is the spin Hall angle.

SHE-generated torques are not capable of explaining their observed angular dependence [21]. The spin drift-diffusion approach must be complemented with the corresponding boundary conditions to include the interplay between the SHE and the interfacial REE. Effects of interfacial spin-orbit interaction on the three-dimensional spin transport at the FL/HM interface at z=0 are conveniently described with the spin-dependent scattering potential $V(\mathbf{r})$ [15], [20]:

$$V(\mathbf{r}) = \frac{\hbar^2 k_F}{m}\delta(z)\left[u_0 I + \boldsymbol{\sigma}\left(u_{ex}\mathbf{m} + u_R\,\mathbf{z}\times\frac{\mathbf{k}}{k_F}\right)\right] \qquad (5)$$

Here u_0, u_{ex}, u_R are the dimensionless magnitudes of the spin-independent potential, the exchange interaction, and the Rashba spin-orbit coupling at the interface, respectively, $\delta(z)$ is the Dirac delta function, k_F is the Fermi wave vector, $\mathbf{k}$ is the wave vector on the Fermi surface, $\boldsymbol{\sigma}$ is the vector of Pauli matrices, m is the effective mass, and $\mathbf{m}$ is the magnetization direction in the ferromagnet at a certain position at the interface.

We employ the finite element method to compute the charge and spin transport on a mesh of a SOT-MRAM. We consider the SHE in HMs and the REE at HM/FM interfaces. With boundary conditions for the interfacial SOC present at HM/FM interfaces, we reproduce the experimentally measured magnitude and non-trivial symmetry of SOTs in Pt/Co [21], as shown in Fig.3.

However, reversing a perpendicular FL deterministically requires an external magnetic field. A promising approach involves leveraging unconventional SOTs in FL/NM/FM trilayers to break this symmetry [19], [22] (Fig.2c). Additional spin currents with out-of-plane spin polarization are generated at the lower NM/FM interface [22] (Fig.4, left), offering the required control over the perpendicular FL magnetization to achieve sub-ns deterministic switching (Fig.4, right).

An alternative path towards generating nonconventional torques due to out-of-plane z-polarized spin currents is to employ noncollinear antiferromagnets (nc-AFMs) as a spin-

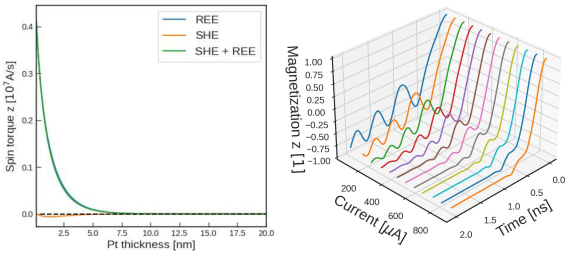

Fig.4 **Left**: Out-of-plane spin current originating from the lower FM/HM interface (Fig.2c). The spin polarization is along z-direction ensuring fast deterministic switching (**right** panel).

polarizing layer in SOT-MRAM devices (Fig.2b). In Mn_3Sn the magnetic spin Hall effect (MSHE) has been reported [23]. As z-polarized spin currents were generated in Mn_3Sn due to the MSHE, the use of nc-AFMs for spin current generation in SOT-MRAM is attractive. We numerically investigated the efficiency of nc-AFMs to generate spin currents with an out-of-plane spin polarization for achieving field-free switching in SOT-MRAM.

Fig.5 (left) displays the spin currents in a Mn_3Sn/FL bilayer. The out-of-plane polarized spin component (green) is substantial within the ferromagnetic FL and, combined with the y-polarized spin current responsible for the damping-like torque, ensures deterministic SOT-induced switching. The magnetic-field free switching with nc-AFM as a spin-polarized current source is predicted to be as fast as the SOT switching assisted with the magnetic field in a conventional HM/FL bilayer (Fig.5, right). In addition, nc-AFMs offer many more functionalities.

Indeed, it has been experimentally demonstrated that Mn_3Sn grown on W with large SHE can be switched between distinct octupole states by means of current-induced spin-orbit torques [24], [25]. Epitaxial tensile strain distorts the Mn_3Sn lattice, breaking the crystal symmetry of the Kagome plane (Fig.6, left). This lifts the six-fold degeneracy and induces a small net magnetic moment $\mathbf{m}_{\text{net}}$ resulting in two stable states, with $\mathbf{m}_{\text{net}}$ pointing either up or down (Fig.6, right).

The direction of the net magnetization $\mathbf{m}_{\text{net}}$ in strained Mn_3Sn on W can be inverted deterministically by applying a charge current to the W layer, if the external magnetic field (of 0.2 T in our simulations) is applied along the x-direction (Fig.6, bottom). Therefore, Mn_3Sn can also be used as a free layer whose state can be electrically manipulated and detected.

If one grows a valve consisting of an out-of-plane CoFeB FL and Mn_3Sn separated by a highly conductive Mo NMS (Fig.7, left), and runs the current in-plane along the

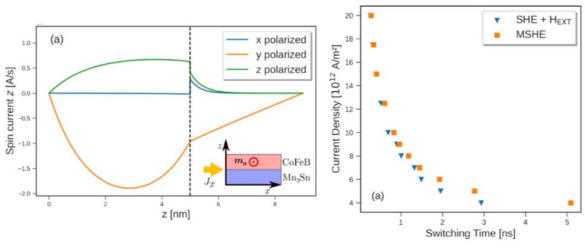

Fig.5 **Left**: Spin current generated in a Mn_3Sn(5 nm)/CoFeB(4 nm) bilayer with a 2×10^{12} Am^{-2} in-plane electric current. **Right**: MSHE-induced switching compared with conventional SOT-MRAM switching assisted by a 60 mT external field along the current direction.

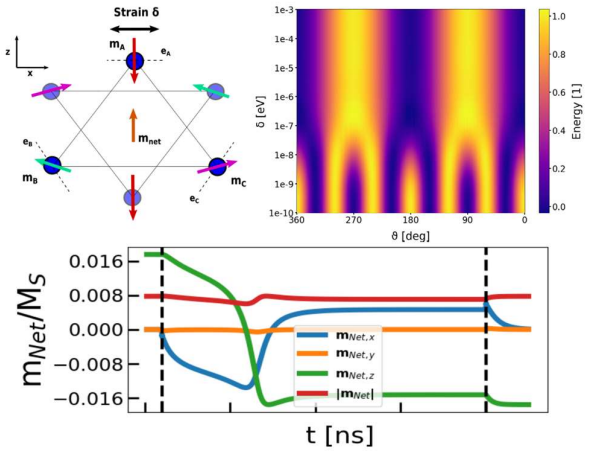

Fig.6 **Left**: Kagome lattice of Mn_3Sn. Applied tensile strain, indicated by δ. **Right**: Increasing the tensile strain results in two stable 'up' and 'down' states. **Bottom**: Net magnetization $\mathbf{m}_{net}$ during switching.

valve, the direction of the ferromagnet can be inverted due to the MSHE in Mn_3Sn. After the FL magnetization $\mathbf{m}_{FM}$ is inverted, the non-conventional torques generated by the spin-orbit interaction at the FL/Mo interface [22] are also reversed and force the net magnetization $\mathbf{m}_{net}$ of Mn_3Sn to flip. The Oersted field generated by a charge current through the structure is sufficient [26] to enable deterministic switching of the Mn_3Sn layer. Fully electric manipulation of the magnetic states in the Mn_3Sn and CoFeB layers is shown in Fig.7, right panel. Leveraging the additional electric control over magnetizations in a Mn_3Sn/Mo/CoFeB trilayer structure is thus promising for future SOT-MRAM devices.

IV. Conclusion

The versatility of the implemented spin and charge coupled transport approach to evaluate the spin-transfer torques acting on ferromagnets in advanced multilayer MRAM cells is demonstrated by treating ultra-fast multilayer STT-MRAM and realistic SOT-MRAM cells. It is shown that nc-AFM Mn_3Sn is promising for emerging devices as a free switching layer. Additional electric magnetization control in a Mn_3Sn/Mo/CoFeB trilayer structure opens exciting perspectives for creating innovative SOT-driven devices.

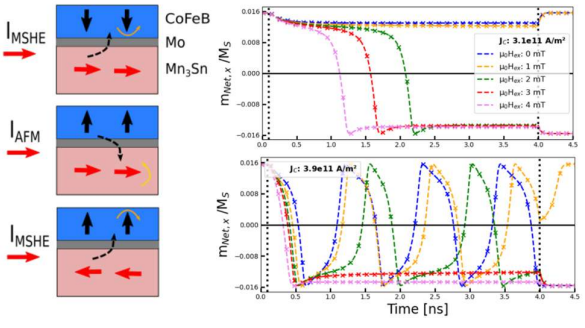

Fig.7 **Left**: Trilayer structure and switching scheme. Red and black arrows indicate $\mathbf{m}_{net}$ and $\mathbf{m}_{FM}$, dotted black arrows indicate the flow of spin current, and orange arrows indicate the rotation of the magnetic moments due to spin. **Right**: calculated x- component of $\mathbf{m}_{net}$ of Mn_3Sn for different magnetic fields and current densities.

Acknowledgment

Financial support by the Austrian Federal Ministry of Labour and Economy, the National Foundation for Research, Technology and Development and the Christian Doppler Research Association is gratefully acknowledged.

References

[1] H. Honjo, K. Nishioka, S. Miura, et al., "25 nm iPMA-type Hexa-MTJ with Solder Reflow Capability and Endurance > 10^7 for eFlash-type MRAM," in Proc. IEDM Conf., pp. 10.3.1-10.3.4 (2022).

[2] T.Y. Lee, M. Lee, M.K. Kim, et al., "World-most Energy-Efficient MRAM Technology for Non-Volatile RAM Applications," in Proc. IEDM Conf., pp.10.7.1-10.7.4 (2022).

[3] S. Ikegawa, K. Nagel, F.B. Mancoff, et al., "High-Speed (400MB/s) and Low-BER STT-MRAM Technology for Industrial Applications", in Proc. IEDM Conf., pp. 10.4.1-10.4.4 (2022).

[4] I S. Ikeda, K. Miura, H. Yamamoto, et al., "A Perpendicular-anisotropy CoFeB–MgO Magnetic Tunnel Junction," Nature Mater. 9, 721 (2010).

[5] H.Sato, M.Yamanouchi, S.Ikeda, et al., "MgO/CoFeB/Ta/CoFeB/MgO Recording Structure in Magnetic Tunnel Junctions with Perpendicular Easy Axis," IEEE Transactions on Magnetics 49, 4437–4440,2013.

[6] J. Slonczewski, "Current-Driven Excitation of Magnetic Multilayers," J. Magn. Magn. Mater. 159, L1-L7 (1996).

[7] L. Berger, "Emission of Spin Waves by a Magnetic Multilayer Traversed by a Current," Phys. Rev.B 54, 9353-9358, 1996.

[8] J. G. Alzate, U. Arslan, P. Bai, et al., "2Mb Array-Level Demonstration of STT-MRAM Process and Performance towards L4 Cache Applications," in Proc. IEDM Conf., pp.2.4.1–2.4.4 (2019).

[9] Y.-D. Chih, C.-C. Chou, Y.-C. Shih et al., "Design Challenges and Solutions of Emerging Nonvolatile Memory for Embedded Applications," in Proc. IEDM Conf., pp.2.4.1–2.4.4 (2021).

[10] https://www.eenewseurope.com/en/tsmc-moves-to-mram-for-scratch-pad-memory/ Accessed on 7.4.2025.

[11] S. Ko, J. Shim, J. H. Park, et al, "Key Technologies of Scaling Embedded MRAM to 8nm Logic and Beyond for Automotive Application", in Proc. IEDM Conf., 2024, pp. 1-4 (2024).

[12] B. Jinnai, J. Igarashi, K. Watanabe, et al., "High-Performance Shape-Anisotropy Magnetic Tunnel Junctions down to 2.3 nm", in Proc. IEDM Conf., pp.24.6.1–24.6.4 (2020).

[13] G. Hu, C. Safranski, J. Sun, et al., "Double Spin-Torque Magnetic Tunnel Junction Devices for Last-Level Cache Applications," in Proc. IEDM Conf., pp. 10.2.1-10.2.4 (2022).

[14] S. Hu, X. Qiu, C. Pan, et al., "Frontiers in All Electrical Control of Magnetization by Spin-Orbit Torque," Journal of Physics: Condensed Matter, vol. 36, no. 25, p. 253001, 2024.

[15] V.P. Amin, P.M. Haney, and M.D. Stiles, "Interfacial Spin–orbit Torques", Journal of Applied Physics, vol. 128, no. 15, p. 151101, 2020.

[16] S. Fiorentini, M. Bendra, J. Ender, et al., "Spin and Charge Drift-diffusion in Ultra-scaled MRAM Cells," Sci.Rep. 12, 20958, 2022.

[17] M. Bendra, R.L. de Orio, S. Selberherr, et al., "Advanced Modeling and Simulation of Multilayer Spin–Transfer Torque Magnetoresistive Random Access Memory with Interface Exchange Coupling," Micromachines 15, 568-1--568-14, 2014.

[18] https://www.iue.tuwien.ac.at/viennaspinmag Accessed on 7.4.2025.

[19] J.Ryu, R. Thompson, J.Y. Park, et al., "Efficient Spin-orbit Torque in Magnetic Trilayers Using All Three Polarizations of a Spin Current," Nat.Electron. 5, pp. 217–223, 2022.

[20] N.P. Jørstad, S. Fiorentini, J. Ender, et al., "Micromagnetic Modeling of SOT-MRAM Dynamics," Physica B: Cond.Mat. 676, 415612, 2024.

[21] K. Garello, I. M. Miron, C. O. Avci, et al., "Symmetry and Magnitude of Spin-orbit Torques in Ferromagnetic Heterostructures," Nat.Nanotechnol. 8, pp. 587–593, 2013.

[22] V. P. Amin, G.G. Baez Flores, A.A. Kovalev, and K.D. Belashchenko, "Direct and Indirect Spin Current Generation and Spin-orbit Torques in Ferromagnet/Nonmagnet/Ferromagnet Trilayers," Phys.Rev.B 110, 214427, 2024.

[23] S. Hu, D.-F. Shao, H. Yan, et al., "Efficient Perpendicular Magnetization Switching by a Magnetic Spin Hall Effect in a Noncollinear Antiferromagnet," Nat.Commun. 13, 4447, 2022.

[24] T. Higo, K. Kondou, T. Nomoto, et al., "Perpendicular Full Switching of Chiral Antiferromagnetic Order by Current," Nature 607, pp. 474 - 479, 2022.

[25] J.-Y. Yoon, P. Zhang, C.-T. Chou, et al., "Handedness Anomaly in a Non-collinear Antiferromagnet Under Spin–orbit Torque," Nat.Materials 22, pp. 1106 – 1114, 2023.

[26] J.-Y. Yoon, Y. Takeuchi, R. Takechi, et al., "Electrical Mutual Switching in a Noncollinear-antiferromagnetic–ferromagnetic Heterostructure." Nat.Commun. 16, 1171, 2025.